RSC Advances

PAPER

View Article Online
View Journal | View Issue

Cite this: *RSC Adv.*, 2021, **11**, 30206

D-Penicillamine functionalized dendritic fibrous nanosilica (DFNS-DPA): synthesise and its application as an innovative advanced nanomaterial towards sensitive quantification of ractopamine†

Milad Baghal Behyar and Nasrin Shadjou *

During the twentieth century, ractopamine (RAC) as one of the important and frequently used feed additives and doping agents has attracted considerable attention in the animal breeding industry and sports competitions. Due to the low metabolism rate of RAC, it is accumulated in livestock tissues. By consuming food, the residues enter the human body causing hazardous side effects including tachycardia, palpitations, and headache. So, sensitive identification of this compound is desirable to combat illicit use and protect food safety. Here, a novel nanomaterial is manufactured based on the functionalization of dendritic fibrous nanosilica with dipenicillamine (KCC-1-NH-DPA). Synthesised advanced nanomaterial was used for the encapsulation of specific DNA-aptamer and incubated on the surface of gold electrode modified by poly(β-cyclodextrin) P(β-CD) which provided the high surface area, excellent mechanical and thermal stability for the dens-loading of encapsulated aptamer. The green platform was provided an efficient apta-platform for the specific recognition of RAC in human biofluids. Electroanalysis of RAC was performed based on "signal ON" protocol. The modified gold electrode by P(β-CD)-(KCC-1-NH-DPA) was used to improve the conductivity and function of the aptasensor towards sensitive identification of RAC in human real sample. Cyclic voltammetry, differential voltammetry, square wave voltammetry, and chronoamperometry techniques were exploited for the measurement of RAC in the concentration range of 0.1 fM to 0.1 mM. Furthermore, the lower limit of quantification (LLOQ) of engineered aptasensor was obtained as 0.1 fM. It is worth noting that the proposed electrochemical aptasensor showed excellent stability, selectivity and performance in standard and human plasma samples. It is important to point out that, synergetic effect of DFNS with high surface to volume, P(β-CD) as conductive substrate and selective aptamer in the fabricated biodevice lead to highly sensitive and selective biosensor for the biomedical analysis of clinical samples. This platform will be provide a new horizon for the application of advanced nanomaterials in biomedical science based POC analysis.

Received 24th July 2021
Accepted 19th August 2021

DOI: 10.1039/d1ra05655g

rsc.li/rsc-advances

1. Introduction

β-Agonists are a class of drugs widely used to treat asthma and lung diseases in medical centers.[1] The function of β-agonists in increasing protein growth and fat loss makes them attractive for use in the livestock industry.[2] Ractopamine (RAC) is one of the most effective agents in helping muscle growth among β-agonists. So, it is widely used in animal nutrition. The large concentrations of β-agonist residues can accumulate in livestock. Due to the fact that β-agonists are very stable, they resist removal and decomposition from biological systems.[3] Owing to human consumption of these animals, β-agonist deposits can be found in the human body. RAC is a significant member of β-adrenergic agonists used in the treatment of respiratory diseases. It can also lead to increased protein accumulation in livestock.[4–6] Therefore, in order to increase muscle growth, it is illegally added to animal feed as an additive. By consuming animal meat by humans, RACs accumulated in animal tissue threaten the health of the consumer and lead to side effects such as muscle tremors, headaches and tachycardia. Several major risks of RAC have been reported, including anxiety, confusion, cardiopalmus, tachycardia, and muscle tremors.[4] RAC has been banned in some countries because of the potential risk to consumers due to its adverse effects, and regulations have been put in place to closely monitor the illegal use of RAC due to the potential for adverse side effects for

Department of Nanotechnology, Faculty of Science and Chemistry, Urmia University, Urmia, Iran. E-mail: n.shadjou@urmia.ac.ir; Tel: +98 44 33363311

† Electronic supplementary information (ESI) available. See DOI: 10.1039/d1ra05655g

consumers.[5] Therefore, sensitive identification of this compound is desirable to combat illicit use and protect food safety.[6]

Currently, various conventional analytical methods for determination of RAC such as liquid chromatography,[7] liquid chromatography-fluorescence,[8] ultra-performance liquid chromatography-tandem mass spectrometry,[9,10] gas chromatography,[11] colorimetry,[12] Raman spectroscopy[13] and electrophoresis[14] were used. Although the mentioned methods are sensitive, most of them are time consuming, costly and always require a professional operator.[15] To solve these problems, aptamer-based electrochemical (EC) sensors promise diagnostics due to their excellent biological detection capability, easy portability, simple pretreatment method and low economic cost.[16,17]

In recent years, an in-depth understanding of nucleic acid aptamers in terms of structural properties and ligand binding has aroused great interest and led to a wide range of cross-sensing methods on aptamer receptors.[18–23] In particular, aptamer-based biosensors have unprecedented advantages over biosensors using natural receptors such as enzymes and antibodies. Scientists have some of idea for the important of aptasensor performance based on application of nano-substrate for the aptamer immobilization and its stability so, nanotechnology plays an important role in the development of biosensors with several unique advantages.[24] Nanomaterials provide many opportunities to regulate the biological function of fusion proteins with attractive applications in analysis due to their excellent advantages such as large surface-to-volume ratios, chemical composition and controllable structures, and various surface properties.[25] Recently, Polshettiwar *et al.*, synthesized low density KCC-1 fiber nanosilica modification.[26] Fibrous dendritic nano silica (DFNS) has excellent applications in biomedicine, biosensing, bioanalysis, energy storage and a variety of adsorbents. One of the unique properties of this wonderful material is the ability to reach the pores of DFNS, which allows you to load drugs, organic metals, metals and organic molecules. In active places without clogging the pores on the silica surface. The DFNS surface can vary from 450 to 1244 $m^2 g^{-1}$ by adjusting their particle size from 40 to 1120 nm and fiber density (number of fibers in a sphere). It should be noted that unlike the distribution of small pore sizes in conventional silica materials, DFNS contains directional radial pores (fibrous channels) and this increases their size from the center of the sphere to the outer surface. DFNS also show excellent stability (chemical, thermal and mechanical) due to having as main elements. The point that seems to be exciting is the low toxicity and biocompatibility of these substances. By controlling the size of these particles, variable properties such as adsorption, dispersion regulation and toxicity can be created in these nano-spheres.[27] NH_2-functionalized KCC-1 has been used as an excellent host for guests such as proteins, enzymes, metals, polymers, peptides and inorganic molecules.[27] The abundance of hydroxyl functional groups in the large surface area of dendrimer fiber nanosilica can improve the surface interaction of DFNS size and the polymer matrix described as hydrogen bonds to prevent DFNS aggregation and fusion.[28–31] In this study, we attempted to use P(β-CD), as an electroconductive layer of biosensor. β-CD is an oligosaccharide composed of seven glucose units that has a toroidal form on the outside of the hydrophilic and a hydrophobic inner cavity. It is well known that β-CD has high excitability and molecular selectivity.[32] Due to the host–guest interaction, different organic, biological and inorganic molecules can be identified through selective binding in the internal cavities of β-CD and create stable host–guest complexes or nanostructured supramolecular assemblies.[33] In the present study, new type of mesoporous silica mateirial (KCC-1 [34–38]) has be used for the biomedical application based on aptasensing strategy.

To the best of our knowledge, aptasensor based on KCC-1-NH_2-DPA has not been reported to detection of RAC till now. Furthermore, high electron transfers property of poly β-cyclodextrin (P(β-CD)), high surface area of KCC-1-NH_2-DPA and high ability of aptamer for capturing of RAC can provide excellent and appropriate platform for determination of RAC in low concentration and load to engineering a high sensitive biosensor for the pharmaceutical analysis. Therefore, we developed a novel and intelligent EC aptasensor for identification of RAC with LLOQ of 0.1 fM by utilizing several advantages of these materials and biomaterials. The designed platform was able to successfully detect RAC in standard and human plasma samples with a wide range of drug concentration.

2. Experimental

2.1 Chemicals and reagents

β-Cyclodextrin (β-CD), valine, *N*-hydroxysuccinimide, 3-aminopropyl triethoxysilane (APTES), 1-ethyl-3-(3-dimethylaminopropyl) carbodiimide, aspartic acid and dipenicillamine (DPA) purchased from Sigma-Aldrich (Ontario, Canada), potassium chloride, potassium ferrocyanide, potassium hexacyanoferrate(III), hexanol, cetyl trimethylammonium bromide (CTAB), tetraethyl orthosilicate (TEOS), ethanol, dried toluene, *N*,*N*-dimethyl sulfoxide (DMSO), glutamic acid, cysteine, cyclohexane, urea were produced by the German company Merck, aptamer (5′-SH-AAA AAG TGC GGGC-3′) purchased from Takapouzist (Tehran, Iran), ractopamine hydrochloride produced by tocris (Bristol, Britain), human plasma samples were obtained from plasma blood transfusion research center (Tabriz, Iran).

2.2 Samples preparation

Human plasma samples are used for assaying the RAC. In this regard, 500 μL of human plasma sample is poured into a 2.0 mL microtubes and spiked with different concentrations of RAC. For protein precipitation, about 500 μL of acetonitrile is added to the desired plasma sample and vortexed for 2 min. The tube contents are centrifuged at 10 000 rpm for 5 min and clear supernatant is transferred to a clean microtubes.

2.3 Apparatus

Electropolymerization and EC measurements were carried out using conventional three electrode system, containing Ag/AgCl as a reference electrode, a platinum wire as an auxiliary electrode and an Au electrode as a working electrode ($d = 2$ mm) in

the EC cell. The electrodes were purchased from Azar electrode and integrated to the Autolab PGSTAT302N which EC system was powered by Nova 1.11 software. Field emission scanning electron microscopy (FE-SEM), (HitachiSU8020, Czech) with an operating voltage of 3 kV provides topographical and elemental information of electrode surface by different magnifications. The elements identification of the electrode was analyzed by an energy dispersive spectroscopy (EDS). KCC-1-NH-DPA was synthesised and characterized (Fig. S1–S6 and Table S1 (see ESI†)) according to our previous report.[27]

2.4 Fabrication of aptasensor

In order to preparation and completely purify the surface of the electrode, first the Au electrode was polished with a fluffy cloth for 2 min. The electrode was then immersed in a solution of dilute sulfuric acid and deionized water in a ratio of 1 : 1 for 10 min. The electrode was then immersed in a 1 : 1 ratio of deionized water and acetone for 5 min. Finally, the electrode was washed and dried at room temperature.

Besides, to further clean the surface of the electrode, the Au electrode was placed in a 50 mM sulfuric acid solution. The cycle continued between the potential of −400 to 1400 mV with a scrolling speed of 100 mV s^{-1} until the voltammograms stabilized (12 cycles).

After cleaning of electrode surface, electropolymerization of β-CD as conductive layer was performed according to our previous report.[39] For more details, 0.005 g of (β-CD) was dissolved in 7 mL of phosphate buffer solution and used for electropolymerization on the surface of the Au electrode by CV technique at a potential range of −1 to 1.5 V with a scan rate of 100 mV s^{-1} (Fig. 1A). Afterward, for the KCC-1-NH_2-DPA electrodeposition on the surface of the Au electrode, 0.01 g of KCC-1-NH_2-DPA was dispersed on deionized water (10 mL) and ChA technique was utilized for the electrodepositing of this nanomaterials on the P(β-CD)/Au electrode (Fig. 1B) which provide high surface area for the dense loading of aptamer. For this purpose, 0.1 g of KCC-1-NH_2-DPA dispersed in 10 mL of deionized water was poured into electrochemical cell and chronoamperogram was recorded in −0.24 V during 100 s. So, KCC-1-NH_2-DPA was deposited on the surface of P(β-CD). Finally, 5 μL of RAC specific aptamer was immobilized on the surface of Au electrode modified by (KCC-1-NH_2-DPA/P(β-CD)) (Scheme 1).

3. Results and discussion

3.1 Morphological characterization of engineered biosensor

FE-SEM and EDS were recorded to analyze the morphology and surface structure of the aptasensor in various fabrication steps. Fig. S7A–H (see ESI†) showed the FE-SEM images of the surface of the electrode modified with the P(β-CD) layer at different scales. According to this figure, polymer film was polymerized on the surface of Au electrode. Fabrication of polymer layer on the surface of electrode was confirmed by EDS which C, O groups was observed. The formed polymer layer increases the surface to volume ration of the electrode which is necessary for the dense loading of aptamer. In is important to point out that, β-CD with their largely hydrophobic cavities of variable size and numerous ways of chemical modification are the subject of intensive electrochemical research including both their behavior in homogeneous solutions and in thin films attached to the electrode surfaces. They provide useful information on the nature of the reduced and oxidized forms of the electroactive compounds such as amino acids, and on the mechanistic aspects of the electrode processes. They also allow monitoring even very subtle changes of the molecular environment of the redox centers by following their redox potentials. Therefore, β-CD are employed in electrochemical sensing devices for the determination of selected analytes. On the other hand, literature review[33] show that, integration of β-CD to the structure of electroactive materials such as carbon quantum dots can be enhancing their electrical conductivity.

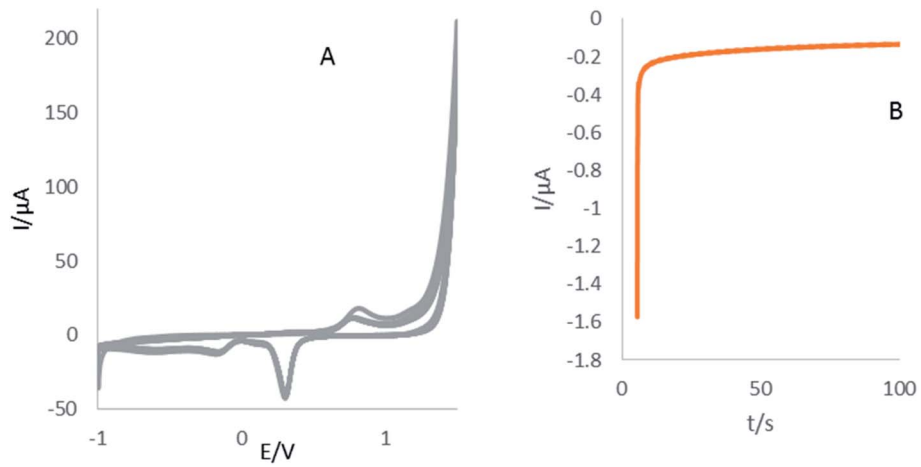

Fig. 1 (A) CVs of Au electrode in the presence of β-CD solution (0.005 g + 7 mL of PBS) at a potential range of −1 to 1.5 V with a scan rate of 100 mV s^{-1}. (B) ChAs of Au electrode modified by P(β-CD) in the presence of KCC-1-NH_2-DPA (0.01 g + 10 mL deionized water) at the potential of −0.24 V during 100 s.

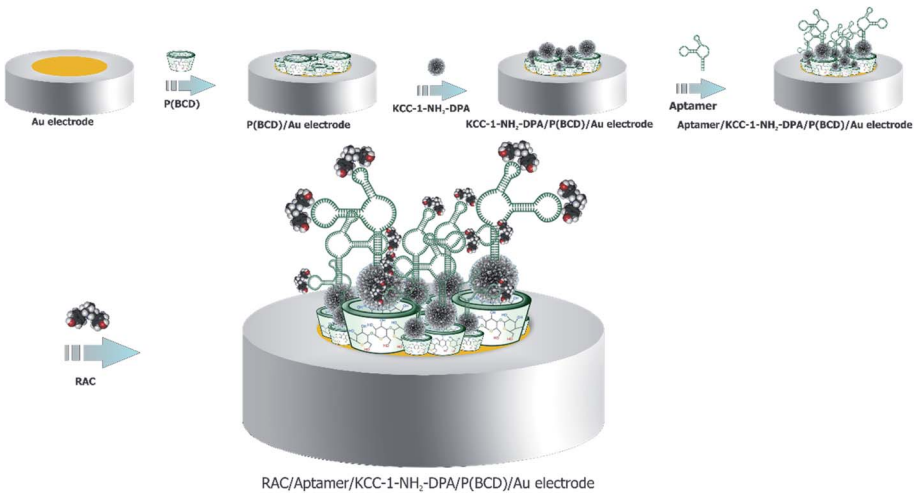

Scheme 1 Illustration of aptasensor for the identification of RAC.

Fig. S8A–H (see ESI†) showed FE-SEM along with EDS of KCC-1-NH_2-DPA on the surface P(β-CD) modified Au electrode (Fig. S14I (see ESI†)). According to the obtained results, the presence of KCC-1-NH_2-DPA layer on the surface of P(β-CD)-Au electrode at different scales was well identified. The structure of KCC-1-NH_2-DPA is a homogeneous layer with the shape of regular spherical grains, which are excellent for efficient loading because they have large pore sizes for loading. Fig. S9A–H (see ESI†) shown FE-SEM images and Fig. S3I† showed EDS of electrode after aptamer immobilization that confirm the existence of aptamer on the surface of KCC-1-NH_2-DPA-P(β-CD)-Au electrode. Finally, Fig. S10A–G (see ESI†) clearly showed the FE-SEM along with EDS analysis of the aptamer/KCC-1-NH_2-DPA-P(β-CD)-Au electrode after interaction with analyte (RAC) at different magnifications. As can be seen, morphology of electrode surface was significantly changed which confirmed interaction of analyte with aptamer sequences. This procedure lead to its detection by redox probe ($[Fe(CN)_6]^{3-/4-}$).

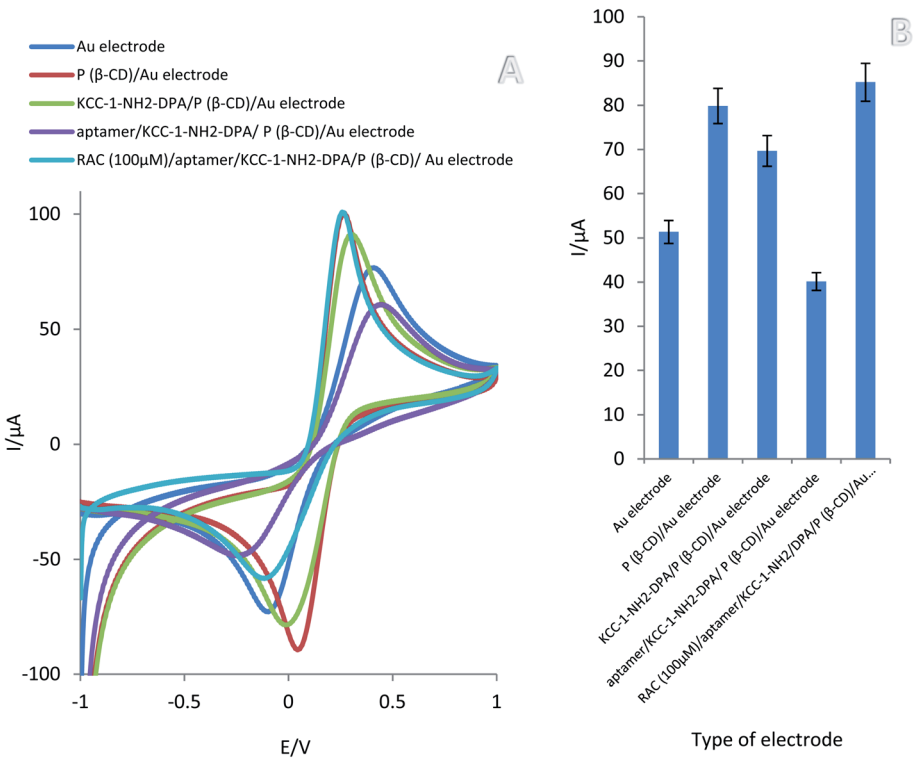

Fig. 2 (A) CVs of Au electrode, P(β-CD)/Au electrode, KCC-1-NH_2-DPA/P(β-CD)/Au electrode, aptamer/KCC-1-NH_2-DPA/P(β-CD)/Au electrode and RAC (100 μM)/aptamer/KCC-1-NH_2-DPA/P(β-CD)/Au electrode in the presence of $[Fe(CN)_6]^{3-/4-}$ 0.01 M + 0.01 M KCl as a support electrolyte at a potential range of −1 to 1 V with a scan rate of 100 mV s^{-1} (B) variation of oxidation peak current *versus* type of electrode. ($n = 3$, SD = 2.14).

3.2 EC evaluation of aptasensor fabrication

CV has become a highly efficient method for electrochemical performance of the modification layers. The steps of aptasensor preparation were determined by CV in 0.01 M $[Fe(CN)_6]^{3-/4-}$/KCl (0.01 M) solution as the supporting electrolyte. Comparison of obtained result demonstrated that polymerization of (β-CD) on the Au electrode have caused increase oxidation peak current from 5.31 to 7.99 μA. Substantially, unique properties of P(β-CD) such as high electrical conductivity on Au electrode led to accelerating electron sharing. These results show the anodic peak current at the surface of P(β-CD) is significantly enhanced while; the cathodic peak current was decreased considerably. These results indicate that P(β-CD) film could accelerate the rate of electron transfer of redox probe ($[Fe(CN)_6]^{3-/4-}$) and have good electrocatalytic activity for redox reaction. Afterward, decorated surface of P(β-CD)/Au electrode with KCC-1-NH_2-DPA caused to decrease peak current from 7.99 to 6.96 μA. This result indicated that the KCC-1-NH_2-DPA was successfully coated on the P(β-CD) matrix, which could delay electron transfer due to poor conductivity candidate silica nanomaterial. After immobilization of the aptamer, the peak current of the electrode was decreased dramatically from to 6.96 to 4.01 μA which confirmed the successful immobilization aptamer on the P(β-CD)-KCC-1-NH_2-DPA. While in this step of sensor preparation, conductivity of total electrode was decrease, but, DFNS could be tap aptamer and increase its stability. Finally, after adding RAC, the peak current increased sharply, which was a good indication of the success of aptasensor designing for the detecting of this analyte by signal ON methodology (Fig. 2A and B).

3.3 Optimization of incubation time of aptamer

The incubation time has a significant role in the performance of aptasensors. For this purpose, the effect incubation time (from 20 min to 1440 min) on the immobilization of aptamer and performance of biosensors engineered was investigated by DPV and ChA techniques in 0.01 M $[Fe(CN)_6]^{3-/4-}$/KCl 0.01 M control solution. According to obtained results, incubation time of 20 min is optimized time for the incubation of aptamer on the surface of KCC-1-NH_2-DPA-P(β-CD)-Au electrode (Fig. S11A–D (see ESI†)).

3.4 Kinetic study

In order to describe the electrochemical performance of modification surface (KCC-1-NH_2-DPA/P(β-CD)/Au electrode), cyclic voltammetry (CV) technique have used for determination of different scan rate effect in the absence of drug (RAC) and in the presence of 0.01 M $[Fe(CN)_6]^{3-/4-}$/KCl as a support electrolyte in the speed range of 0.1 to 1 mV s^{-1} (Fig. S12A (see ESI†)). As shown in Fig. S12C (see ESI†), the linear regression equation can be written as $I_{pa}(\mu A) = 5.18\nu^{1/2}(V\ s^{-1}) + 17.35$ ($R^2 = 0.9867$). A linear relationship between I_{pa} and the square root of the scan speed indicated that mass transfer controlling the process of oxidation occurred *via* diffusion (Fig. S12C (see ESI†)). In addition, there is a linear relationship between ln I_{pa} and ln ν that can be seen in the following equation:

$$\text{Ln } I_{pa}\ (\mu A) = 0.4434 \ln \nu\ (V\ s^{-1}) + 2.1556\ (R^2 = 0.9859).$$

A slope of 0.4434 showed that the electrode process was almost completely controlled by diffusion (Fig. S12E (see ESI†)). A slope of about 0.5 is predicted for diffusion-controlled electrode processes and a slope of close to 1 is predicted for adsorption-controlled processes.[45]

We used the following equation to calculate the number of electrons transferred from the anode potential peak *versus* the Neperian logarithm of sweep rate;[45]

$$E_p = \left(\frac{n^2 F^2}{4RT}\right) \ln \nu + \text{constant}$$

The transferred electrons for the designed aptasensor was $n = 1$.

In the next step, using the following equation, it can be shown that the linear flow peaks up to the scan speed can be explained by examining that the surface redox pairs have electrochemical activity.

$$I_p = \left(\frac{n^2 F^2}{4RT}\right) \nu A \Gamma^*$$

where Γ^* covers the surface of redox species, R-universal gas constant (8.314 J K^{-1} mol^{-1}), F-Faraday constant (96 487 C mol^{-1}), T Kelvin temperature (298 K), ν (sweep rate) and A is the surface area of the electrode ($A = 0.0314$ cm^2). Γ^* is obtained:

$$\Gamma^* = 4.5249 \times 10^{-6}\ \text{mol cm}^{-2}$$

Also, the value of the electron transfer coefficient (α) for the reaction can be calculated from the following equation:

$$E_p = \left(\frac{RT}{2\alpha F}\right) \ln \nu + \text{constant}$$

The anode potential peak relationship with the potential scan rate logarithm (Fig. S12D (see ESI†)) Γ^* indicated that the value of the electron transfer coefficient was equal to $\alpha = 0.4012$. Therefore, this value has proved the irreversible nature of the electrode diffusion process.

Therefore, in order to reach the best state of the nano-aptasensor construction, 20 min was selected as the optimum incubation time in this apta-assay.

3.5 Analytical approach

DPV and SWV techniques were used to detection of different concentrations of RAC (0.1 fM to 0.1 mM) in 0.01 M $[Fe(CN)_6]^{3-/4-}$ 0.01 M + 0.01 M KCl solution. Fig. S13A–D (see ESI†) demonstrated DPVs and SWVs of fabricated aptasensor with the corresponding calibration curve for various concentrations of RAC. As can be seen, well defined peaks have been clearly achieved in the range of 0.1 fM and 0.1 mM of RAC. Furthermore, there is a direct relationship between the concentration of RAC and the peak current. Based on the obtained resulted,

the linear range and LLOQ of developed aptasensor were 0.1 fM to 0.1 mM and 0.1 fM, respectively. Also, calibration curves plotted the linear regression equation to DPVs and SWVs are as follows:

Linear regression equation obtained from DPV evaluation in standard samples:

$$I_p\ (\mu A) = 0.6989 \log C_{(RAC)} + 8.9838,\ R^2 = 0.9443$$

Linear regression equation obtained from SWV evaluation in standard samples:

$$I_p\ (\mu A) = 2.0814 \log C_{(RAC)} + 27.018,\ R^2 = 0.937$$

The analytical performance of previously reported biosensors for determination of RAC was compared with our fabricated biosensor (Table 1).

Up to now, many EC biosensors with different support materials such as carbon, silica and magnetic nanomaterials have been reported for the detection of RAC. According to Table 1, it is obvious that proposed aptasensor shows better analytical performance than other developed biosensors. As can be seen, the linear range obtained by engineered bio-device was wider than most of the reported EC biosensors of RAC. Other advantages of developed EC aptasensor were superior in identification of RAC due to four important causes. Satisfactory results can be attributed to important reasons: (1) the presence of P(β-CD) polymer layer with a unique high electron transfer property which led to faster detection of RAC. (2) The presence of a layer of mesoporous silica nanomaterials (KCC-1), which greatly increased the surface area and created a higher site for high aptamer loading on the surface of the modified electrode. (3) suitable sequence of aptamer with, which makes the prepared apta-platform more selective than other sensors. (4) Suitable preparation of aptasensor under a fast, simple and economical process as other benefits of this protocol can help build aptasensor at a lower cost.

3.6 Evaluation of selectivity

Reliability is one of essential and fundamental factor which has been investigated by specificity and selectivity of fabricated analytical approaches. For this purpose, CV, SWV and ChA techniques were used to selectivity evaluation of prepared aptaassay (Fig. S14, see ESI†). Different interferers including glutamic acid, aspartic acid, L-cysteine and valine were utilized instead of RAC which $[Fe(CN)_6]^{3-/4-}$ 0.01 M + 0.01 M KCl was supporting electrolyte. Based on Fig. S14A–G,† the redox signals of apta-platform for RAC (0.0001 M) detection was compared with the responses of interfering species by similar aptasensor.

According to the results in terms of current intensity, RAC had the highest current intensity, which means that disturbing species have low involvement in the detection of RAC and this analyte was detectable in suitable manner which, the peak current of RAC, glutamic acid, aspartic acid, L-cysteine and valine were 6.23, 4.06, 4.15, 4.85, and 4.42 μA, respectively in CVs. Also, the results showed that the analyte potential was lower than all the interferers, which means that the engineered aptasensor acted quite selectively in detecting the target drug (RAC). Similar results were obtained by SWV and ChA techniques.

3.7 Reproducibility and stability of fabricated aptasensor

In order to evaluate the performance of the developed aptasensor (aptamer/KCC-1-NH_2-DPA/P(β-CD)/Au electrode), stability and reproducibility were evaluated by CV technique in the potential range of −1 V to +1 V and scan rate of 100 mV s^{-1}. The reproducibility was studied by 3 similar electrodes (aptamer/KCC-1-NH_2-DPA/P(β-CD)/Au electrode) under same conditions in 0.01 M $[Fe(CN)_6]^{3-/4-}$/KCl 0.01 M solution. Obtained results demonstrated that the aptasensor designed under the same conditions showed satisfactory repeatability (Fig. S15A and B (see ESI†)). Also, cyclic stability, intra-day and inter-day of designed aptasensor were evaluated by recording CVs of electrode. In order to evaluation of the cyclic stability of the electrode substrate, 100 consequents CVs (1, 5, 10, 50, and 100) was operated. According to the obtained results the peak currents of shows no decrease by increasing number of cycles (Fig. S16A and B (see ESI†)). In addition, the intraday stability of the fabricated aptasensor was measured by measuring the peak current after storing the electrodes at 4 °C for 4 days that the aptasensor shows 98% stability after use, which showed the good performance and stability of our developed platform (Fig. S17 (see ESI†)). But, after 72 h its stability was decreased so, this aptasensor is stable for 48 h.

Table 1 Comparison of analytical performance of developed aptasensor with other reported EC biosensors for the determination of RAC

Strategy	Detection technique	Linear range (μmol L^{-1})	Limit of detection (μmol L^{-1})	Reference
GO/GCE[a]	DPV	0.074–2.96	0.056	40
G/GNR/GCE[b]	DPV	0.001–2.7	0.00051	41
MWCNT/MIM/SPE[c]	DPV	0.02–0.2	0.006	42
MWCNT/GCE[d]	DPV	0.148–5.92	0.059	43
CNPs/GCE[e]	DPV	0.002–0.03	0.0002	44
Aptamer/KCC-1-NH_2-DPA/P(β-CD)/Au electrode	CV, DPV, SWV and ChA	1×10^2–1×10^{-10}	1×10^{-10}	This work

[a] GO modified GCE. [b] Graphene/gold nanorod modified GCE. [c] Multi-wall carbon nanotubes and molecularly imprinted membranes modified screen-printed electrode. [d] Multi-wall carbon nanotubes modified GCE. [e] Carbon nanoparticle modified GCE.

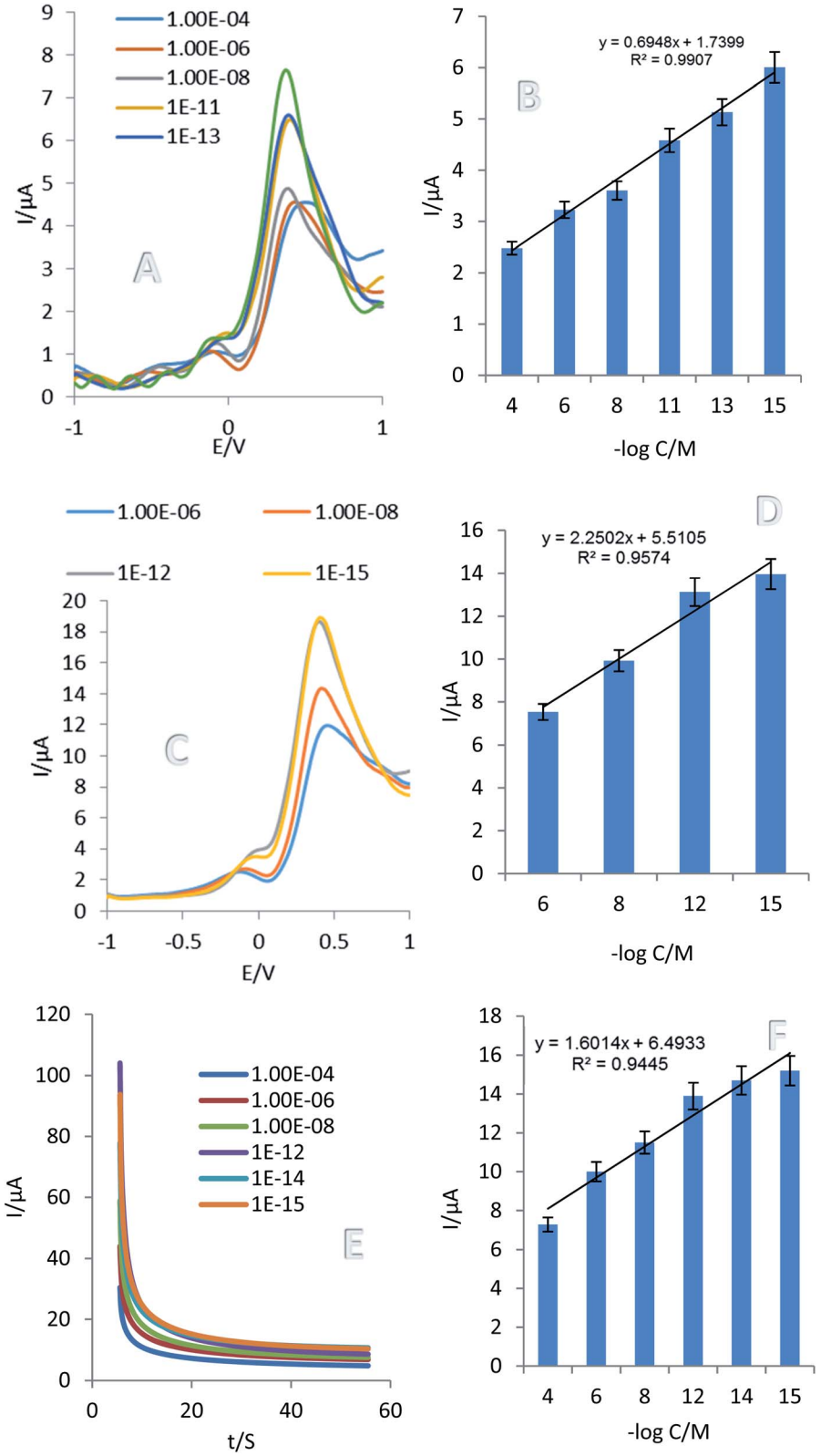

Fig. 3 DPVs (A), SWVs (C) and ChAs (E) of different concentrations of RAC (10^{-4}, 10^{-6}, 10^{-8},10^{-12}, 10^{-14} and 10^{-15} M) with human plasma samples were recorded in the potential range −1 to 1 V and the scan rate of 100 mV s^{-1} in the potential range of control electrolyte $[Fe(CN)_6]^{3-/4-}$ 0.01 M + KCl 0.01 M and calibration curves ((B), (D), and (F) for DPV, SWV and ChA, respectively). (n = 3, SD = 2.25 for CV), (n = 3, SD = 2.29 for DPV), and (n = 3, SD = 2.36 for ChA).

3.8 Analysis of real plasma samples

In order to evaluation of designed aptasensor performance in real sample and its practical application, different concentrations of RAC (10^{-4} M, 10^{-6} M, 10^{-8} M, 10^{-12} M, 10^{-14} M and 10^{-15} M) were added to human plasma samples and mixed well. After 10 min, the supernatant was collected and 5 μL were dropped on the surface of the prepared aptasensor. DPV, SWV and ChA techniques were used for the analytical evaluation in real sample (Fig. 3). Also 0.01 M $[Fe(CN)_6]^{3-/4-}$/KCl 0.01 M solution was selected as the support electrolyte to determine the amount of RAC in the human plasma sample. According to the obtained results the linear concentration range was 0.1 fM to 1 mM which LLOQ is 1 fM. The results demonstrated that there is a good linear relationship between RAC concentration (log C) and peak current. The regressions equation achieved as follows; the linear regression equation was obtained from the DPV calculation in the plasma sample:

$$I_p\ (\mu A) = 0.6948 \log C_{RAC} + 1.7399,\ R^2 = 0.9907$$

The linear regression equation was obtained from the SWV calculation in the plasma sample:

$$I_p\ (\mu A) = 2.2502 \log C_{RAC} + 5.5105,\ R^2 = 0.9574$$

The linear regression equation was obtained from the ChA calculation in the plasma sample:

$$I_p\ (\mu A) = 2 \times 10^6 \log C_{RAC} + 6 \times 10^6,\ R^2 = 0.9445$$

Based on calibration curves in human plasma sample, it is proved that proposed aptasensor is proved that proposed aptasensor is applicable for suitable analysis of real samples.

4. Conclusion

In summary, an innovative EC aptasensor based on KCC-1-NH_2-DPA-P(β-CD)/Au electrode was successfully designed for sensitive and selective recognition of RAC in real samples. Proposed aptasensor showed a suitable linear detection range, excellent sensitivity, which related to high surface area of DFNS, and appropriate electron transfer capability. This aptasensor had features such as good reproducibility, high stability and exclusive response to RAC in the presence of other interfering agents. The calibration curves were linear than various concentration of RAC in the range of 0.1 fM to 0.1 mM, which LLOQ was 0.1 fM. This newly designed aptasensor was also studied with different concentrations of RAC in human plasma with a concentration range of 0.1 fM to 0.1 mM which LLOQ was 0.1 fM, and showed its capabilities in biomedical applications. Future of prepared aptasensor could have great potential for applications in testing quality control of livestock products as well as human health monitoring in clinical laboratories and hospitals. It is also recommended to detect different analytes and to develop the sensor as an on-site detection sensor to expand this research.

Author contributions

Milad Baghal Behyar: methodology, analysis data, investigation, writing–review and editing. Nasrin Shadjou: project administration, investigation, funding acquisition, methodology, supervision, resources, writing–review and editing.

Conflicts of interest

There are no conflicts to declare.

Acknowledgements

We appreciate the Urmia University to support of this study.

References

1 C. Crescenzi, S. Bayoudh, P. Cormack, T. Klein and K. Ensing, *Anal. Chem.*, 2001, **73**, 2171–2177.
2 Y. Xiong, M. Gower, C. Li, C. Elmore, G. Cromwell and M. Lindemann, *Meat Sci.*, 2006, **73**, 600–604.
3 S. Carr, D. Hamilton, K. Miller, A. Schroeder, D. Fernández-Dueñas, J. Killefer, M. Ellis and F. McKeith, *Meat Sci.*, 2009, **81**, 533–539.
4 G. Brambilla, T. Cenci, F. Franconi, R. Galarini, A. Macrı, F. Rondoni, M. Strozzi and A. Loizzo, *Toxicol. Lett.*, 2000, **114**, 47–53.
5 D. Smith, *J. Anim. Sci.*, 2000, **78**, 2903–2912.
6 Y. Zhou, Y. Yang, X. Deng, G. Zhang, Y. Zhang, C. Zhang, S. Shuang, Y. He and W. Sun, *Sens. Actuators, B*, 2018, **276**, 204–210.
7 C. Li, Y.-L. Wu, T. Yang, Y. Zhang and W.-G. Huang-Fu, *J. Chromatogr. A*, 2010, **1217**, 7873–7877.
8 E. I. Shishani, S. C. Chai, S. Jamokha, G. Aznar and M. K. Hoffman, *Anal. Chim. Acta*, 2003, **483**, 137–145.
9 M. Nielen, J. Lasaroms, M. Essers, J. Oosterink, T. Meijer, M. Sanders, T. Zuidema and A. Stolker, *Anal. Bioanal. Chem.*, 2008, **391**, 199–210.
10 B. Shao, X. Jia, J. Zhang, J. Meng, Y. Wu, H. Duan and X. Tu, *Food Chem.*, 2009, **114**, 1115–1121.
11 L. Wang, Y.-Q. Li, Y.-K. Zhou and Y. Yang, *Chromatographia*, 2010, **71**, 737–739.
12 Y. Zhou, P. Wang, X. Su, H. Zhao and Y. He, *Talanta*, 2013, **112**, 20–25.
13 F. Zhai, Y. Huang, C. Li, X. Wang and K. Lai, *J. Agric. Food Chem.*, 2011, **59**, 10023–10027.
14 L. Shen and P. He, *Electrochem. Commun.*, 2007, **9**, 657–662.
15 J. Du, B. Zhu, X. Peng and X. Chen, *Small*, 2014, **10**, 3461–3479.
16 A. Hayat, A. Sassolas, J.-L. Marty and A.-E. Radi, *Talanta*, 2013, **103**, 14–19.
17 R. Thota and V. Ganesh, *Sens. Actuators, B*, 2016, **227**, 169–177.
18 S. L. Clark and V. T. Remcho, *Electrophoresis*, 2002, **23**, 1335–1340.
19 T. Mairal, V. C. Özalp, P. L. Sánchez, M. Mir, I. Katakis and C. K. O'Sullivan, *Anal. Bioanal. Chem.*, 2008, **390**, 989–1007.

20 S. Tombelli, M. Minunni and M. Mascini, *Biosens. Bioelectron.*, 2005, **20**, 2424–2434.
21 I. Willner and M. Zayats, *Angew. Chem., Int. Ed.*, 2007, **46**, 6408–6418.
22 H. K. Kordasht, M. Pazhuhi, P. Pashazadeh-Panahi, M. Hasanzadeh and N. Shadjou, *TrAC, Trends Anal. Chem.*, 2020, **124**, 115778.
23 T. Hermann and D. J. Patel, *Science*, 2000, **287**, 820–825.
24 N. Li, X. Su and Y. Lu, *Analyst*, 2015, **140**, 2916–2943.
25 Z. Zhang, Y. Zhang, R. Song, M. Wang, F. Yan, L. He, X. Feng, S. Fang, J. Zhao and H. Zhang, *Sens. Actuators, B*, 2015, **211**, 310–317.
26 N. Bayal, B. Singh, R. Singh and V. Polshettiwar, *Sci. Rep.*, 2016, **6**, 1–11.
27 M. Mahmudi, N. Shadjou and F. A. M. Hasanzadeh, *J. Electroanal. Chem.*, 2019, **848**, 113272.
28 N. P. Patel, A. C. Miller and R. J. Spontak, *Adv. Mater.*, 2003, **15**, 729–733.
29 N. P. Patel, A. C. Miller and R. J. Spontak, *Adv. Funct. Mater.*, 2004, **14**, 699–707.
30 N. C. Su, Z. P. Smith, B. D. Freeman and J. J. Urban, *Chem. Mater.*, 2015, **27**, 2421–2429.
31 X. Yang, L. Yan, F. Ran, A. Pal, J. Long and L. Shao, *J. Membr. Sci.*, 2019, **576**, 9–16.
32 G. T. Selvan, S. Poomalai, S. Ramasamy, P. M. Selvakumar, I. V. Muthu Vijayan Enoch, S. G. Lanas and A. Melchior, *Anal. Chem.*, 2018, **90**, 13607–13615.
33 M. Shanmugam, D. Ramesh, V. Nagalakshmi, R. Kavitha, R. Rajamohan and T. Stalin, *Spectrochim. Acta, Part A*, 2008, **71**, 125–132.
34 K. AbouAitah, A. Farghali, A. Swiderska-Sroda, W. Lojkowski, A. Razin and M. Khedr, *J. Nanomed. Nanotechnol.*, 2016, **7**, 1.
35 S. M. Sadeghzadeh, *Microporous Mesoporous Mater.*, 2016, **234**, 310–316.
36 H. K. Kordasht and M. Hasanzadeh, *J. Mol. Recognit.*, 2020, **33**, e2832.
37 S. Ge, Y. Zhang, L. Zhang, L. Liang, H. Liu, M. Yan, J. Huang and J. Yu, *Sens. Actuators, B*, 2015, **220**, 665–672.
38 S. M. Sadeghzadeh, *Catal. Commun.*, 2015, **72**, 91–96.
39 M. Hasanzadeh, S. Hassanpour, A. S. Nahr, N. Shadjou, A. Mokhtarzadeh and S. Mahboob, *Anal. Bioanal. Electrochem.*, 2018, **10**, 77–97.
40 C. Wu, D. Sun, Q. Li and K. Wu, *Sens. Actuators, B*, 2012, **168**, 178–184.
41 W. Bai, H. Huang, Y. Li, H. Zhang, B. Liang, R. Guo, L. Du and Z. Zhang, *Electrochim. Acta*, 2014, **117**, 322–328.
42 H. Zhang, G. Liu and C. Chai, *Sens. Actuators, B*, 2012, **168**, 103–110.
43 Z. Liu, Y. Zhou, Y. Wang, Q. Cheng and K. Wu, *Electrochim. Acta*, 2012, **74**, 139–144.
44 S. Yao, Y. Hu, G. Li and Y. Zhang, *Electrochim. Acta*, 2012, **77**, 83–88.
45 E. A. Hillard, F. C. de Abreu, D. C. M. Ferreira, G. Jaouen, M. O. F. Goulart and C. Amatore, *Chem. Commun.*, 2008, 2612–2628.